Mechanism of Folding of the Dimeric Core Domain of *Escherichia coli Trp* Repressor: A Nearly Diffusion-Limited Reaction Leads to the Formation of an On-Pathway Dimeric Intermediate†

Lisa M. Gloss‡ and C. Robert Matthews*

Department of Chemistry and Center for Biomolecular Structure and Function, Pennsylvania State University, University Park, Pennsylvania 16802

Received June 25, 1998; Revised Manuscript Received September 8, 1998

ABSTRACT: A polypeptide corresponding to the core/dimerization domain of *E. coli Trp* repressor (TR), $[2-66]_2$ TR, was constructed by insertion of a pair of stop codons into the *trpR* gene. The kinetic properties of the urea-induced folding of this core fragment were examined by intrinsic tryptophan fluorescence (FL) and circular dichroism (CD) spectroscopy. The kinetic response of wild-type TR (WT TR) is very complicated and has been interpreted to involve three parallel channels with multiple folding and isomerization reactions (Mann et al. (1995) *Biochemistry 34,* 14573−14580). The refolding of $[2-66]_2$ TR can be described by a much simpler mechanism, involving an association reaction followed by a urea-dependent first-order folding reaction. The second-order rate constant for the association reaction approaches that of the diffusion limit, 3×10^8 M^{-1} s^{-1} in 1 M urea at 15 °C. Double-jump experiments demonstrate that ≥93% of the unfolded monomers proceed to the native dimer via the dimeric intermediate; several lines of evidence demonstrate that this dimeric species is an on-pathway intermediate. The subsequent first-order folding reaction of the dimeric intermediate to the native species involves development of additional secondary structure and tertiary structure. The kinetic folding mechanism of $[2-66]_2$ TR suggests that: (1) the complexity of the folding kinetics of full-length WT TR arises from alternative interactions of the DNA reading heads with the dimerization core domain—not from the intertwined nature of the dimerization interface; (2) residues 2−66 contain all of the sequence information necessary to direct the near-diffusion-limited association reaction in a TR folding reaction; and (3) the formation of secondary and tertiary structure is concurrent with or precedes dimerization, and further development certainly follows the formation of quaternary structure.

The oligomeric nature of many proteins plays an essential role in the maintenance of homeostasis in a cell, in functions as diverse as metabolism, energy production, and cell division as well as transcription and its regulation. There are regulatory advantages to the evolution of multimeric structures, such as allosteric control mechanisms (e.g., aspartate transcarbamolyase and lactate dehydrogenase), cooperativity in ligand binding (e.g., hemoglobin and DNA-binding proteins), rate enhancement of sequential steps in metabolic pathways (e.g., *E. coli* tryptophan synthase and fatty acid synthase), or very precise control of DNA replication and transcription (e.g., DNA and RNA polymerase complexes). Elucidation of the regulation of function via quaternary structure in multimeric systems requires biophysical characterization of the formation and stability of oligomeric proteins.

A major goal of molecular biophysics is to understand how the amino acid sequence of a protein codes for the efficient transformation of a random coil, unfolded state into a unique three-dimensional structure characteristic of the native, functional form. Although many insights have been gained into folding mechanisms by the study of monomeric proteins (for reviews, see refs *1*−*3*), less is understood about how the development of quaternary structure is coordinated with the formation of secondary and tertiary structure during folding reactions. The folding pathways of some oligomeric proteins have been reported (reviewed in ref *4*). However, improved time resolution and protein engineering have permitted the elucidation of more detailed mechanisms for several dimeric systems, including the P22 *Arc* repressor (*5, 6*) and the β_2 subunit of *Trp* synthase (*7, 8*). These two examples span a range of complexities in their folding responses from the simple two-state mechanism of the single-domain P-22 *Arc* repressor to multiple transient intermediates detected in the folding of the multidomain β_2 *Trp* synthase dimer.

The coordination of the various levels of structural organization is a particularly fascinating issue for the *E. coli Trp* repressor (*9*−*11*). *Trp* repressor (TR^1) is a prototypical member of the helix-turn-helix family of DNA-binding proteins. Each monomer of 107 residues contains six α-helices (*12, 13*). The A−C helices of each monomer are intimately intertwined to form the hydrophobic core and dimerization domain of TR (Figure 1). The DE and D′E′

† Supported by National Institutes of Health (NIH) Grant GM 54836 to C.R.M. L.M.G. was supported in part by an NIH Postdoctoral Fellowship GM 16685.

* To whom correspondence should be addressed.

‡ Present address: Department of Biochemistry and Biophysics, Washington State University, Pullman, WA 99164-4660.

10.1021/bi981511p CCC: $15.00
Published on Web 10/23/1998

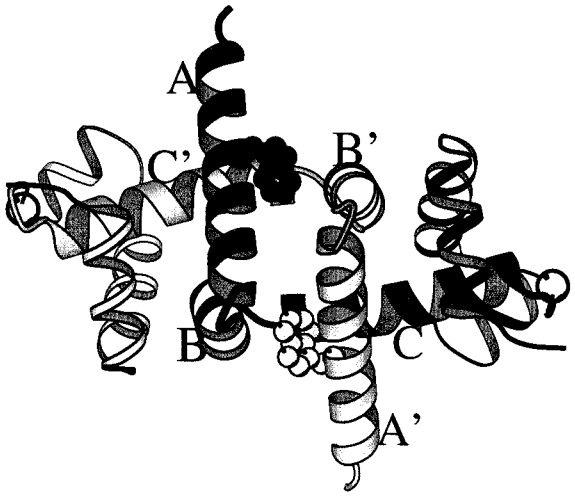

FIGURE 1: Ribbon diagram of full-length WT *Trp* repressor from the X-ray crystal structure (*12*). The $[2-66]_2$ TR variant spans helices A, B, C, A′, B′, and C′, shown in the wider ribbons; the terminal residues, 66 and 66′ are indicated by the large white spheres. The single tryptophan remaining in core fragment, Trp-19, is shown. This figure was generated using Molscript v1.4 (*54*).

helices are the DNA-reading heads and extend outward from the core domain. The terminal F helices are docked against the core domain and contribute additional inter-monomer contacts with the A and B helices of the other monomer.

The folding of WT TR, reversibly induced by urea, is a two-state equilibrium process (*9*). The proposed kinetic folding mechanism, however, is much more complicated (*14*, *15*). The burst-phase reaction of WT TR leads to the formation of a monomeric intermediate, detectable by SF-CD and SF-FL of ANS. Further folding proceeds through three parallel channels; protein in each channel undergoes a dimerization step and an isomerization step. Previous studies on a des-Pro TR demonstrated that none of the channels, nor the isomerization reactions, are caused by proline isomerization reactions (*15*). The kinetic complexity of multiple channels for TR folding might arise from two possibilities: different docking modes between the DNA-reading heads and the ABC core or different arrangements of the core helices in an early folding event. One means of addressing these different explanations is to examine the folding of the isolated core/dimerization domain. If the multiple channels arise from alternative structures within the core (A, B, C, A′, B′, and C′ helices), a polypeptide fragment corresponding to the core sequence should fold by a mechanism similar to that of full-length TR. Conversely, if the alternative pathways are a product of interactions between the core and the DNA-reading heads, truncation of the protein should greatly simplify the folding mechanism.

Characterization of proteins simplified by producing fragments corresponding to putative subdomains has provided useful insights into the structure/function relationship of full-length proteins (e.g., refs *16*−*18*). Fragmentation methodology has also been applied directly to the study of protein folding to produce stable models for transient kinetic intermediates or autonomously folding substructures in order to elucidate the folding pathway (e.g., refs *19*−*23*).

The structural properties of a TR core fragment, corresponding to residues 8−71 generated by chymotryptic cleavage, have been reported (*24*). Subsequently, a second generation core fragment was engineered by stop codon mutagenesis; the sequence of this fragment, $[2-66]_2$ TR, was selected to more precisely correspond to the secondary structure boundaries seen in the full-length structure. The equilibrium unfolding properties for the reversible thermal and urea denaturation of the $[2-66]_2$ TR have been reported (*25*). In the current study, fragmentation yielded a much simpler folding mechanism which elucidates some of the complexities of the folding of full-length TR.

MATERIALS AND METHODS

Materials. Ultrapure urea was purchased from ICN Biomedicals Inc. All other chemicals were of reagent grade. The expression and purification of the $[2-66]_2$ TR fragment has been described elsewhere (*25*). WT TR was expressed and purified as previously described (*26*).

Methods. (a) CD and Fluorescence Spectroscopy. The buffer conditions for the kinetic folding experiments were 10 mM potassium phosphate, 0.1 mM ethylenediamine tetraacetic acid (EDTA), pH 7.6 with varying concentrations of ultrapure urea. The drive trains used for the collection of most of the kinetic data were BioLogic SFM-3 stopped-flow (SF) modules. For SF-FL, the light source and detection units were also BioLogic instruments; for SF-CD, the drive train was interfaced with an AVIV 62DS spectrophotometer (*14*). The dead time of the BioLogic SF instruments was ∼5 ms, with cuvette path lengths of 1.5 and 2 mm. Initially, SF-FL and SF-CD data were collected for 50 s, demonstrating that there were no slow kinetic responses occurring on a time scale longer than 10 s. Subsequently, data were collected over two time ranges; the fastest regime spanned the first 1 s of the folding or unfolding reaction ($\Delta t = 1$ ms) with an instrumental time constant of 1 ms. Data were also collected for longer times, 2−10 s ($\Delta t = 2$ to 10 ms) with an instrumental time constant of 2−5 ms. To enhance the signal-to-noise ratio, multiple shots were averaged; 4−10 shots were averaged for a typical SF-FL trace, and 30−50 shots were averaged for far-UV SF-CD data. SF-CD data were collected at 222 nm; for SF-FL data, the excitation wavelength was 295 nm, and emission was detected after a 320 nm cutoff filter. Typical protein concentrations were 3.5−15 μM monomer.

The refolding of $[2-66]_2$ TR was also monitored by SF-FL using ANS, with excitation at 370 nm, and emission was detected after a 460 nm cutoff filter. The data were collected in two ways. (1) Standard refolding jumps were made from 6 M urea to 1 M urea, with final concentrations of 7 μM monomer and 42 μM ANS. (2) Protein was refolded to 1 M urea (7 μM monomer) in the absence of ANS; after various folding delays, ANS in 1 M urea was pulsed into the reaction, yielding a final concentration of 5.6 μM monomer.

To determine an association rate constant, SF-FL data (of intrinsic Trp FL) were collected at sub-micromolar monomer

[1] Abbreviations: $[2-66]_2$ TR, dimeric *Trp* repressor fragment containing residues 2−66; ANS, 8-anilino-1-naphthalenesulfonate; CD, circular dichroism; C_M, the urea concentration at which the apparent fraction of unfolded monomer constitutes 50% of the population; FL, fluorescence; k_{XY}, the rate for the transformation of X species to Y species; MRE, mean residue ellipticity; SF, stopped flow; TR, *Trp* aporepressor; WT, dimeric wild-type *Trp* aporepressor containing residues 2−108.

concentrations. These experiments employed an Applied Photophysics SFM 17 MV stopped-flow instrument. The dead time was ~6 ms with a path length of 2 mm. The excitation wavelength was changed to 285 nm to enhance the fluorescence signal, and the bandwidth was 9.3 nm. A set of 20−30 shots was averaged per kinetic trace.

(b) Data Analysis. Individual kinetic traces were fit locally with the Macintosh version of KaleidaGraph 3.0 (Abelbeck Software) to an equation of an exponential form:

$$Y(t) = Y_\infty + \sum_{i=1}^{N} Y_i \exp(-t/\tau_i) \quad (1)$$

where Y_i is the amplitude of the kinetic phase and Y_∞ is the equilibrium signal of the sample. The $[2-66]_2$ TR data were adequately described by fits to a single-exponential term. WT data required a sum of three exponential terms (*9*, *14*).

$[2-66]_2$ TR data were also analyzed with the global fitting routine, Savuka 5.0, an in-house software program (*27*). These analyses permitted the simultaneous fitting of multiple data sets collected by CD and FL under varying conditions of urea, monomer concentration, and temperature. The urea dependencies of the relaxation times were fitted to the equation

$$\frac{1}{\tau_i} = k^{H_2O} \exp\left\{\frac{m^{\ddagger}[\text{Urea}]}{RT}\right\} \quad (2)$$

where k^{H_2O} is the rate constant of the folding or unfolding reaction in the absence of urea and $m^{\ddagger}$ reflects the sensitivity of the reaction to denaturant. Equation 2 was used to fit the urea dependence of the relaxation times obtained from fits of individual traces to eq 1, as well as to fit globally multiple SF-FL and SF-CD traces over a range of urea concentrations; similar results were obtained by both methods.

RESULTS

$[2-66]_2$ TR Refolding Involves First- and Second-Order Processes. Refolding and unfolding reactions were monitored by two optical methods: SF-CD at 222 nm to assess α-helical content and SF-FL to monitor development of tertiary and quaternary structure around Trp-19 in $[2-66]_2$ TR. A representative refolding SF-CD trace for $[2-66]_2$ TR is shown in Figure 2A. At 25 °C and monomer concentrations above 0.25 μM, the refolding response of $[2-66]_2$ TR by SF-CD and SF-FL is well-described by a single exponential, with similar relaxation times for both methods. The relaxation times display a dependence on urea concentration (Figure 3A) that is typical of protein folding reactions (*28*); however, they are independent of monomer concentration. For example, at 2.0 M urea, the observed relaxation time, from SF-FL and SF-CD, is 0.15 ± 0.01 s, from 3.0 to 15 μM monomer (data not shown), demonstrating that this folding reaction is a first-order process. The single-exponential response of $[2-66]_2$ TR is far simpler than that observed for WT TR (*9*, *14*), which requires three exponentials to adequately describe the data (Figure 3B).

To test whether the observed kinetic phases account for the entire folding process, the SF-CD amplitudes can be compared to the ellipticity observed at equilibrium for the native and unfolded species. For the unfolding of $[2-66]_2$ TR, the total amplitude change detected by equilibrium titrations for the $N_2 \rightleftharpoons 2U$ transition is observed in a single-exponential response (data not shown); there is no evidence for a very rapid unfolding reaction occurring in the dead time of the stopped-flow instrument. In contrast, the ellipticity observed after the first 5 ms of refolding is substantially greater than that expected for unfolded [2−66] monomers at 1 M urea (indicated by the upper arrow in Figure 2). The relative percent of the dead-time signal increases with monomer concentration from 3.5 to 15 μM; this suggests that the dead-time reaction may be a second-order dimerization reaction. The final ellipticity reached after refolding of $[2-66]_2$ TR (Figures 2, 5, and 6) agrees very

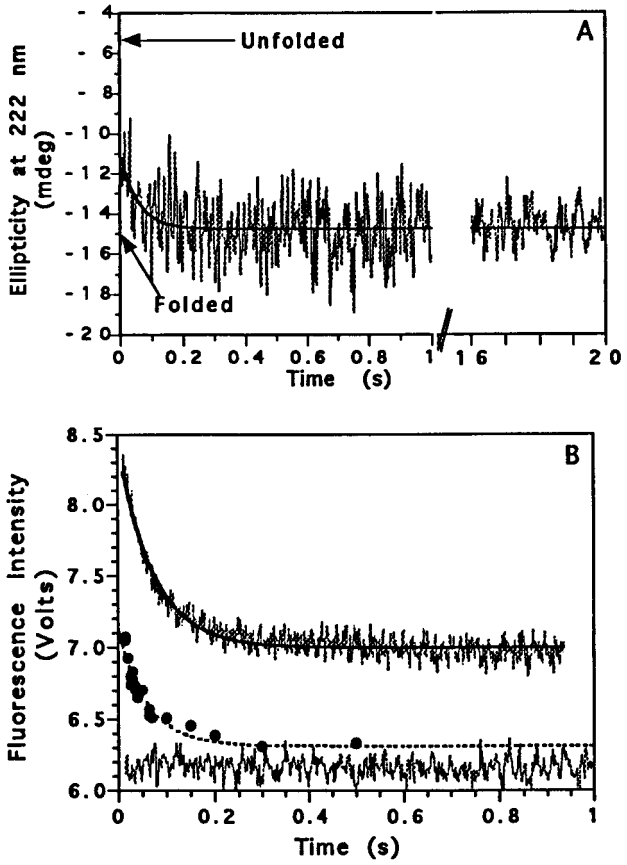

FIGURE 2: Representative refolding kinetic responses of $[2-66]_2$ *Trp* repressor under strongly refolding conditions. The protein was denatured in 6 M urea and refolded to 1.0 M urea. The lines are fits to a single-exponential phase. (A) Stopped-flow circular dichroism refolding response at 7 μM monomer. The arrows indicate the ellipticity of folded and unfolded $[2-66]_2$ TR at 1.0 M urea, the latter extrapolated from the linear base line observed at high urea concentrations. (B) Refolding response monitored by ANS using stopped-flow fluorescence. The upper kinetic trace is the refolding of $[2-66]_2$ TR in the presence of 42 μM ANS (7 μM monomer). The solid line is the fit of the data to a single exponential, yielding a relaxation time of 76 ± 3 ms. The lower kinetic trace is the fluorescence of 42 μM ANS alone in 1 M urea. The initial fluorescence observed when 42 μM ANS is pulsed into the sample after various folding delays is also shown (●); the dotted line represents the fit of these data to a single exponential with the relaxation time fixed at that seen for SF-CD and tryptophan SF-FL under similar conditions, 60 ms. For the pulsed experiment, the protein was refolded to 7 μM monomer but diluted to 5.6 μM by the addition of ANS. The fluorescence intensity was not corrected for this difference in monomer concentration. Conditions: 25 °C, 10 mM potassium phosphate, 0.1 mM EDTA, pH 7.6.

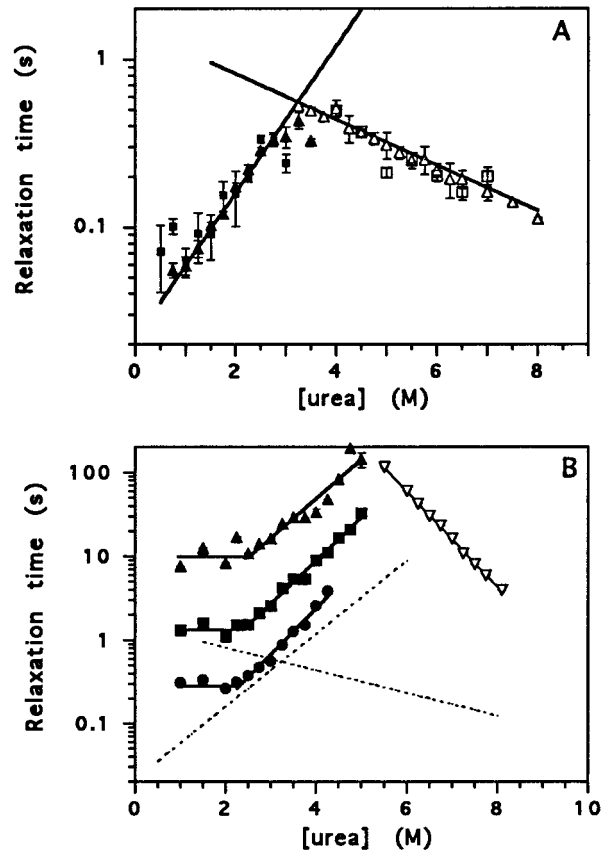

FIGURE 3: Refolding and unfolding kinetics of $[2-66]_2$ TR and WT TR monitored by stopped-flow fluorescence and circular dichroism. (A) Urea dependence of the apparent refolding and unfolding relaxation times of $[2-66]_2$ TR at 7 μM monomer. The fits of the SF-FL (■, □) and SF-CD (▲, △) data to a single exponential are shown for folding (filled symbols) and unfolding (open symbols). The solid lines represent global fits of the data to eq 2. (B) Urea dependence of the three kinetic refolding phases (▲, ■, ●) and the single unfolding phase (△) of WT TR at 5.6 μM monomer. The data points represent simultaneous fits of SF-FL and SF-CD traces at a given urea concentration. The solid lines are fits to an exponential dependence of the relaxation time on urea concentration (eq 2); for the folding data, the exponential dependence is described by two regimes, 1.0−2.5 M with essentially no urea dependence ($m \sim 0$) and from 2.5 to 5 M urea, with a strong urea dependence ($m \sim 1$). For comparison, the fitted lines for $[2-66]_2$ TR (panel A) are included as dotted lines. Conditions are as described in Figure 2. Error bars are indicated or are equivalent to the size of the symbols.

well with that expected from equilibrium urea denaturation (*25*).

The burst-phase and subsequent first-order folding reaction can also be monitored by SF-FL with ANS (Figure 2B). This hydrophobic dye binds to the folding protein in the 5 ms dead time and then is dissociated from the protein with a relaxation time that is similar to that observed by SF-FL and SF-CD of intrinsic probes. The binding and dissociation of ANS were monitored by two methods. Kinetic traces were collected with ANS in the refolding buffer (upper trace in Figure 2B). In other systems, this method has yielded artifacts induced by refolding in the presence of a hydrophobic ligand (*29*). To verify that the binding of ANS in the burst-phase was not a dye-induced artifact, ANS was also pulsed in after various folding delays, and the SF-FL amplitudes were monitored as a function of folding delay (data points is Figure 2B). Both methods gave similar kinetic responses for the observed folding reaction. The relaxation time monitored by SF-FL in the presence of ANS was 76 ± 3 ms, compared to relaxation times of 59 and 63 ms for intrinsic tryptophan SF-FL and SF-CD, respectively (Figure 3A). The slightly slower rate measured by ANS FL may reflect a retardation due to the energetic cost of removing ANS from exposed hydrophobic surfaces. These data demonstrate that nonpolar surfaces have coalesced in the dead-time intermediate and are buried in the rate-limiting step of folding. The residual ANS fluorescence signal (Figure 2B) suggests that there are ANS binding sites in the folded, dimeric core, presumably on the exposed hydrophobic surface upon which the D−F helices dock in the full-length protein.

Using the intrinsic fluorescence change of Trp-19, refolding data could be collected at sub-micromolar protein concentrations. At 25 °C and 0.25 μM monomer, the SF-FL refolding response was well-described by a single first-order process. To be completed in the SF dead time, the second-order rate constant must be $\geq 5 \times 10^8$ M^{-1} s^{-1}. Between 7 and 17 °C and with monomer concentrations of 0.1−0.4 μM, a second process was apparent (left half of Figure 4). Unlike the slow first-order process, the relaxation time of this faster folding reaction is clearly dependent on monomer concentration (Figure 4).

Detection of this association reaction by SF-FL confirmed that the intermediate formed in the SF-CD dead time is dimeric. Unfortunately, the urea dependence of this reaction could not be characterized. At urea concentrations less than 1 M, the reaction was too fast to monitor accurately; at urea concentrations greater than 1 M, the amplitude became vanishingly small. This implies that at sub-micromolar monomer concentrations, the dimeric intermediate is only marginally stable.

$[2-66]_2$ TR Folds by a Very Rapid Association Reaction. The kinetic traces at 15 °C (1 M urea) shown in Figure 4 were fitted globally to the model

$$2\,U \underset{k_{IU}}{\overset{k_{UI}}{\rightleftharpoons}} I_2 \underset{k_{NI}}{\overset{k_{IN}}{\rightleftharpoons}} N_2 \qquad (3)$$

to extract values for the second-order rate constant, k_{UI}. This analysis requires knowledge of the unfolding rate constants. The value of k_{NI} at 15 °C was fixed at a value determined in a companion study (0.33 s^{-1}; the following paper in this issue). The value of k_{IU} was either treated as an adjustable parameter or fixed at values 5−10 times that of k_{NI}; the value of k_{UI} did not vary significantly with the various choices of k_{IU}. As unfolding of $[2-66]_2$ TR proceeds by a single-exponential process with no burst-phase reaction (traces not shown), it was assumed that the $N_2 \rightarrow I_2$ reaction was rate-determining. The global fit of the data gave an association rate constant of $(3 \pm 1) \times 10^8$ M^{-1} s^{-1}. The value of this rate constant is enhanced at 25 °C and at lower urea concentrations. Its temperature dependence (see the following paper in this issue) predicts a rate of 7×10^8 M^{-1} s^{-1} at 25 °C and 1 M urea (Table 1).

The Dimeric Intermediate Is Remarkably Stable. To determine the stability of the dimeric intermediate, the dead-time amplitudes of SF-CD data, at micromolar monomer concentrations (Figure 2), were examined as a function of urea. The validity of this analysis rests upon the very rapid

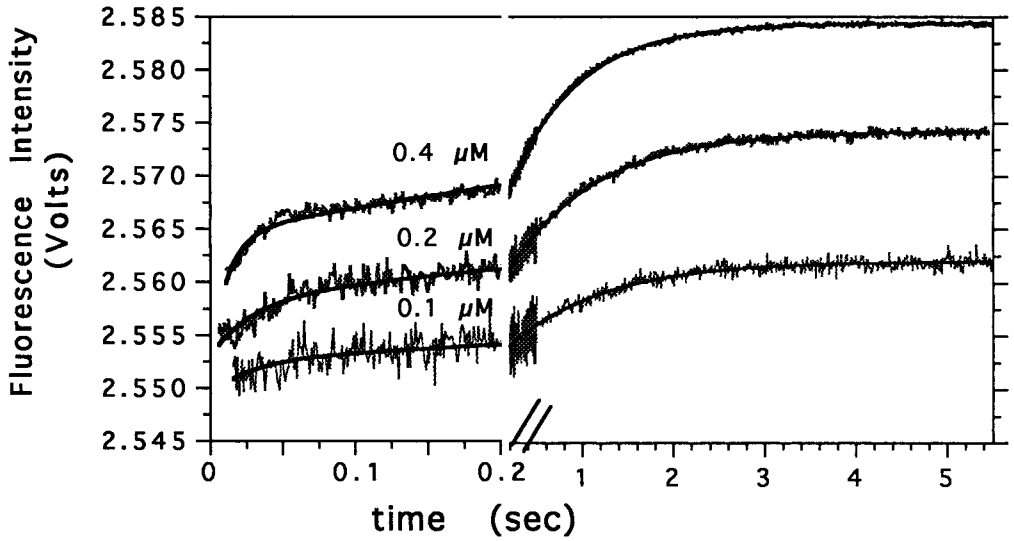

FIGURE 4: Stopped-flow fluorescence refolding traces of $[2-66]_2$ TR under conditions where the second-order dimerization reaction can be detected. The traces are the average of 20−30 shots. The solid lines are derived from fitting the data to a $2U \rightleftharpoons I_2 \rightleftharpoons N_2$ model. Conditions: 15 °C, 1 M urea final, 0.1−0.4 μM monomer, 10 mM potassium phosphate, 0.1 mM EDTA, pH 7.6.

Table 1: Kinetic and Thermodynamic Parameters Describing the Folding and Unfolding Reactions of the $[2-66]_2$ TR at 25 °C[a]

Kinetic Parameters					
reacn		fitting method		k_{UI} (M^{-1} s^{-1})	
$2U \rightarrow I_2$		global fit[b]		7×10^8 (1×10^8)	
		k_{IN} (H_2O) (s^{-1})	$m^{\ddagger}_{IN}$ (kcal mol^{-1} M^{-1})	k_{NI} (H_2O) (s^{-1})	$-m^{\ddagger}_{NI}$ (kcal mol^{-1} M^{-1})
$I_2 \rightleftharpoons N_2$	local fits[c]	40.8 (4.0)	0.571 (0.024)	0.625 (0.043)	0.194 (0.009)
	global fit[c]	46.4 (0.2)	0.595 (0.001)	0.651 (0.005)	0.185 (0.001)
Thermodynamic Parameters					
			$\Delta G°(H_2O)$ (kcal mol^{-1})		m (kcal mol^{-1} M^{-1})
$I_2 \rightleftharpoons N_2$	local[d]		2.48 (0.48)		0.77 (0.07)
	global[d]		2.53 (0.03)		0.78 (0.01)
$2U \rightleftharpoons I_2$	global[e]		10.3 (0.3)		1.20 (0.08)
$2U \rightleftharpoons N_2$	kinetics		12.8 (0.5)		1.98 (0.15)
	equilibrium[f]		13.3 (0.2)		2.00 (0.05)

[a] Standard errors are given in parentheses. Folding and unfolding kinetics were monitored by SF-FL and SF-CD. [b] This rate constant represents a global fit of SF-FL data at sub-micromolar concentrations (Figure 4) at 1 M urea and 15 °C and is extrapolated to 25 °C on the basis of the temperature dependence to be reported elsewhere (following paper in this issue). [c] These values represent the fitted parameters for SF-FL and SF-CD data collected at 25 °C and a monomer concentration of 7 μM (data are shown in Figure 3A). the individual kinetic traces were fitted locally to a single exponential (eq 1), and the resulting relaxation times fitted to an exponential urea dependence (eq 2) to obtain values for $m^{\ddagger}$ and $k(H_2O)$. SF-FL and SF-CD data at several urea concentrations (0.5−3.5 M for folding, 84 traces; and 4.5−8 M for unfolding, 20 traces) were also fit globally to eq 2. [d] Calculated from the kinetic data using eqs 4a,b. [e] The stability was determined from the SF-CD amplitudes determined from the global fitting to eq 2 of SF-FL and SF-CD data at 7 and 15 μM monomer (84 and 59 traces, respectively). Data are shown in Figure 5. [f] Reference *25*. The $\Delta G°(H_2O)$ value is ∼10% lower than that reported previously for global fitting of the equilibrium data. the FL data had been converted to intensity-averaged emission wavelength (*50*); however, that quantity does not necessarily provide an accurate description of thermodynamic parameters. the data have been refitted using single-value decomposition (*51*−*53*), resulting in the value given in Table 1.

formation of this species prior to its conversion to the N_2 conformer (*30*). SF-FL and SF-CD data were collected at 25 °C at 7 and 15 μM monomer. The data set was comprised of 84 traces at 7 μM, including 25 SF-CD traces, and 59 traces at 15 μM, including 23 SF-CD traces. These data were globally fitted to eq 2; the amplitudes of N_2 and the $I_2 \rightarrow N_2$ reaction (Y_∞ and Y_i, respectively, in eq 1) were not linked over all data sets but rather were treated as adjustable local parameters for each trace. The urea dependence of the SF-CD amplitudes is shown in Figure 5. The final amplitudes for both protein concentrations agreed well with those expected from equilibrium urea titrations, demonstrating the complete reversibility of the folding of $[2-66]_2$ TR. The midpoint of the unfolding transition, C_M, of the dead-time intermediate is dependent on monomer concentration: 2.9 and 3.3 M urea for the 7 and 15 μM data sets, respectively. The dead-time amplitudes for the 7 and 15 μM data were globally fitted to the model $2U \rightleftharpoons I_2$, with the unfolded base line fixed at the values obtained from equilibrium data and the folded base lines linked between the two data sets. This analysis yielded values for $\Delta G°(H_2O)$ of 10.3 ± 0.3 kcal mol^{-1} and an m value of 1.20 ± 0.08 kcal mol^{-1} M^{-1} (Table 1).

The Dimeric Intermediate Contains Helical Structure. SF-CD kinetic traces, refolding to concentrations of 1 M urea and 7 μM monomer, were collected as a function of wavelength. The wavelength dependencies of the dead-time and final amplitudes are shown in Figure 6. For comparison, equilibrium spectra of $[2-66]_2$ TR at 1 and 6 M urea (unfolded) are also shown. The final amplitudes agree very

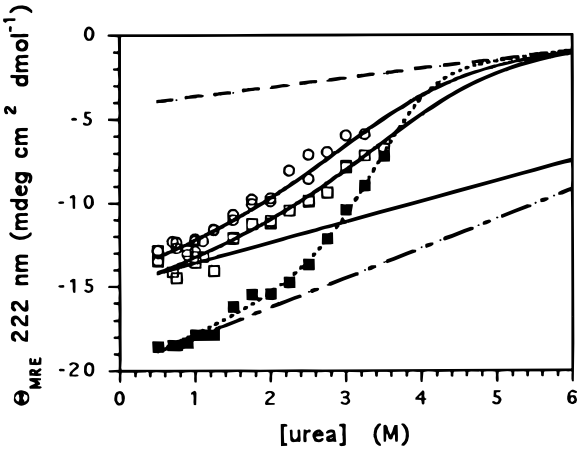

FIGURE 5: Urea dependence of the stopped-flow circular dichroism amplitudes for the refolding of $[2-66]_2$ TR. Data were collected at 7 and 15 μM monomer (circles and squares, respectively). The amplitudes developed during the stopped-flow dead time, 5 ms, are presented as open symbols. The solid lines are fits of the dead-time amplitudes to a $2U \rightleftharpoons I_2$ model, showing both the native base line of I_2 and the unfolding transition. The final amplitude of the 15 μM data is also included (■); the 7 μM final amplitude data were omitted for clarity. The nonsolid lines represent data collected by equilibrium CD: short-dash line, the unfolding transition; dotted−dashed line, the folded base line; long-dash line, the unfolded base line which was fixed in the fitting of the dead-time amplitudes. Conditions are given in the legend of Figure 2.

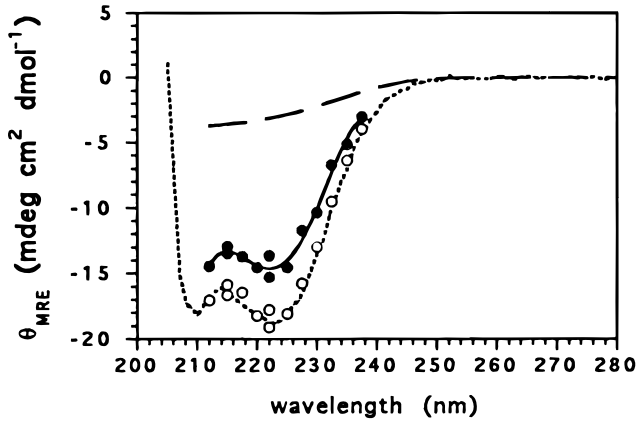

FIGURE 6: Circular dichroism spectrum of the dimeric intermediate observed in the folding reaction of $[2-66]_2$ TR. SF-CD kinetics were monitored as a function of wavelength at final conditions of 1 M urea and 7 μM monomer. The dead-time and final amplitudes are represented by ● and ○, respectively. Equilibrium spectra, collected at 1 M urea (dotted line) and 6 M urea (initial conditions, dashed line) are also shown. The solid line through the dead-time data is drawn to guide the eye. Absorption of light by 1 M urea precluded the collection of data below 212 nm. Conditions as in Figure 2.

well with the 1 M urea spectrum. The dead-time amplitudes exhibit a wavelength dependence typical of a partially helical protein and are similar in shape to that observed for the native dimer, though with ~20% less ellipticity from 212 to 238 nm.

I_2 Is an Obligatory Intermediate. From the SF-CD data, it is clear that a significant fraction of the ensemble of unfolded monomers folds to a dimeric intermediate in less than 5 ms at micromolar concentrations. It is conceivable, however, that this intermediate is not obligatory, i.e., that some fraction of unfolded protein can fold directly to the native dimer without transiently populating any intermediates.

Scheme 1: Possible Folding Mechanisms for $[2-66]_2$ TR

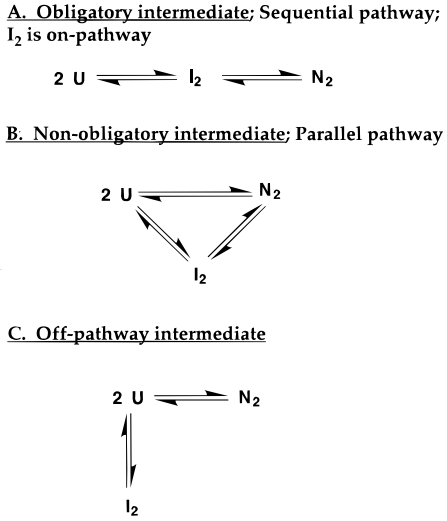

These two alternatives are diagrammed in Scheme 1A,B, and could be termed sequential or parallel mechanisms, respectively.

Under favorable circumstances, these two mechanisms can be distinguished by a double-jump experiment. The unfolded protein is allowed to fold for varying lengths of time, and then the unfolding reaction of the protein is monitored. When τ_{delay} is less than the observed relaxation time for the folding reaction, the population of the N_2 species may be different for the two mechanisms. For a parallel pathway (Scheme 1B), the amount of N_2 formed is proportional to the relative rate constants for the formation of I_2 and N_2 from U. If folding proceeds by a sequential pathway (Scheme 1A), the formation of N_2 will be constrained by the rate-determining step in refolding. If I_2 is an obligatory intermediate, the amplitude of the unfolding reaction should approach zero as τ_{delay} approaches the dead time of the stopped flow. This assumes that I_2 unfolds more rapidly than N_2, a valid assumption for $[2-66]_2$ TR (see above).

SF-FL double-jump kinetics at 25 °C showed that the unfolding amplitude decreased with decreasing delay time, suggesting that I_2 is an obligate species for the majority of the protein molecules (data not shown). However, the relaxation time of $I_2 \rightleftharpoons N_2$ is sufficiently rapid that it was difficult to determine if the intermediate was absolutely obligatory. At this temperature, ~10% of the protein was expected to fold completely to N_2, via I_2, at even the shortest accessible delay times (6 ms).

To decrease the rate of the $I_2 \rightleftharpoons N_2$ reaction, double-jump kinetics were also performed at 15 °C. The results of a SF-FL experiment, in which unfolded $[2-66]_2$ TR was folded to 1.5 M urea for varying delay times and then unfolded, are shown in Figure 7. The rate of unfolding, after τ_{delay}, was similar to that measured for the direct unfolding of N_2 under similar conditions (3 μM monomer, 1.5−6 M urea, 15 °C). The refolding rate observed from the time dependence of the unfolding amplitude in the double-jump experiment (fitted line in Figure 7) is 3.4 ± 0.1 s^{-1}. This value is in excellent agreement with that determined by standard methods under the same conditions, 3.49 ± 0.01 s^{-1}. The unfolding amplitude extrapolated to $\tau_{delay} = 0$ is 7 ± 5% of the total unfolding amplitude detected at very long delay times. Similar results were obtained by SF-FL when

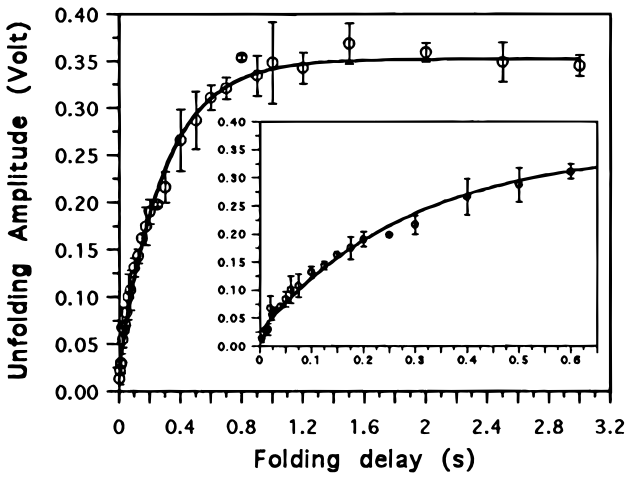

FIGURE 7: Stopped-flow fluorescence double-jump experiment on $[2-66]_2$ TR. The protein was unfolded in 6 M urea, refolded to 1.5 M urea and 7 μM monomer for varying time periods, and then unfolded to 5 M urea. The amplitude detected for the unfolding reaction is plotted as a function of the folding delay time. The data points and error bars represent the average value of 3−6 traces per delay time and the standard deviation of the amplitude locally fitted for the multiple traces. Conditions: 3 μM final monomer concentration, 15 °C, 10 mM potassium phosphate, 0.1 mM EDTA, pH 7.6.

the protein was refolded to 2 M urea (data not shown). SF-CD double-jump experiments gave ~5% amplitude remaining when τ_{delay} approached zero (data not shown). These results make it clear that the great majority of protein folds through the dimeric intermediate. The small remaining unfolding amplitudes may arise from a small contribution from the unfolding reaction for the I_2 species or a small fraction of "fast-track" folding directly to native (*32*).

The $I_2 \rightleftharpoons N_2$ Reaction of $[2-66]_2$ TR at 25 °C. A single $m^{\ddagger}$ value describes the urea dependence of the first-order folding reaction of $[2-66]_2$ under both strongly and weakly refolding conditions (Figure 3A), in contrast to the urea dependence of the WT TR refolding kinetics (Figure 3B). The refolding relaxation times of WT are independent of urea concentration up to ~2.5 M (i.e., the $m^{\ddagger}$ value as described in eq 2 is ~0) (*9, 14*). The relaxation times are urea-dependent above 2.5 M, with an $m^{\ddagger}$ value of ~1. The unfolding kinetics of both WT TR and $[2-66]_2$ TR are well-described by a single exponential and depend on the urea concentration in an exponential manner (eq 2).

The rate constants and the $m^{\ddagger}$ values describing the folding and unfolding reactions of $[2-66]_2$ TR at 25 °C are given in Table 1, with good agreement between local and global fits. The $\Delta G°(H_2O)$ and m value for the $I_2 \rightleftharpoons N_2$ reaction can be calculated from the data presented in Figure 3A and Table 1, with the following relationships:

$$\Delta G°(H_2O) = -RT \ln\left\{\frac{k_{NI}(H_2O)}{k_{IN}(H_2O)}\right\}$$

$$m = m^{\ddagger}_{IN} - m^{\ddagger}_{NI} \quad (4a,b)$$

where k^{H_2O} and $m^{\ddagger}$ are defined as in eq 2. This reaction contributes 2.5 kcal mol^{-1} to the free energy of folding of $[2-66]_2$ TR with an m value of 0.78. From the thermodynamic values given in Table 1 for the $2U \rightleftharpoons I_2$ and the $I_2 \rightleftharpoons N_2$ reactions, a total $\Delta G°(H_2O)$ and m value for the $2U \rightleftharpoons N_2$ reaction of $[2-66]_2$ TR can be determined. As shown in Table 1, the thermodynamic parameters determined from kinetics methods agree well with those previously determined by equilibrium methods (*25*). This agreement supports the choice of the simple sequential folding model (Scheme 1A).

The similarity of the N_2 species to the transition state for the $I_2 \rightleftharpoons N_2$ reaction can be estimated from the value of α (*33*):

$$\alpha = \frac{m^{\ddagger}_{IN}}{m^{\ddagger}_{IN} - m^{\ddagger}_{NI}} \quad (5)$$

For the folding of the dimeric intermediate of $[2-66]_2$ TR, the value of α is 0.76. The value of α can range from 0 to 1, describing the position of the transition state relative to the intermediate and native species (1 being completely nativelike). The α value of $[2-66]_2$ TR suggests that transition state between I_2 and N_2 is quite nativelike with respect to burial of surface area.

DISCUSSION

Folding Mechanism of $[2-66]_2$ TR. The folding of $[2-66]_2$ TR involves two well-resolved kinetic steps: (1) a very rapid association reaction and (2) a first-order folding reaction. From double-jump experiments (Figure 7) it is clear that >95% of the folding molecules transiently populate a dimeric intermediate.

The possibility that the remaining ~5% amplitude observed in the double-jump experiments could reflect a small population of N_2 forming directly from U in the stopped-flow dead time (Scheme 1B) can be ruled out on the basis of other kinetic and thermodynamic data. The rate of $2U \rightarrow N_2$, estimated from the relative flux through the pathways diagrammed in Scheme 1B, as determined from the double-jump data, should be 1/20th the rate of $2U \rightarrow I_2$, or ~5×10^7 M^{-1} s^{-1} at 25 °C. Given this rate constant and that of $k_{unf}(H_2O)$ (0.625 s^{-1} at 25 °C; Table 1), the $\Delta G°(H_2O)$ for $2U \rightleftharpoons N_2$ should be ~10 kcal mol^{-1}. This stability is substantially less than that determined from equilibrium methods, 13.3 ± 0.2 kcal mol^{-1} (*25*). Furthermore, this would necessitate that N_2 is metastable with respect to I_2 ($\Delta G°(H_2O)$ = 10.3 kcal mol^{-1}; Table 1 and Figure 5). The agreement between the final CD amplitudes and the equilibrium data (Figure 5) clearly shows that N_2, not I_2, is the more stable species and the final state observed in the folding process. The ~5% amplitude seen in the double-jump experiments probably arises from a small contribution from the unfolding reaction for the I_2 species.

Two classes of intermediates may arise in protein folding: on-pathway intermediates—those which must be transiently populated during the folding process of a protein, leading to the final native species—and off-pathway intermediates—those which must unfold before proceeding to the native species. These alternatives are diagrammed in Scheme 1A,C.

An off-pathway mechanism would require that the observed first-order reaction in stopped-flow folding experiments is actually an unfolding reaction of $I_2 \rightarrow 2U$, followed by a non-rate-determining dimerization reaction to form N_2. The positive $m^{\ddagger}$ value observed for the first-order reaction in the folding of $[2-66]_2$ TR is not consistent with such an

unfolding reaction (Table 1, Figure 3A). The $m^{\ddagger}$ value of a reaction is thought to be proportional to the amount of the surface area change occurring between the initial species and transition state of the reaction (*31*). A positive $m^{\ddagger}$ value indicates a *burial* of surface area, typical of a folding reaction; unfolding reactions generally proceed with a negative $m^{\ddagger}$ value. Such negative values are seen for the unfolding of off-pathway intermediates; two examples are the dissociation of a nonnative histidine ligand from the heme moiety in the folding of cytochrome *c* (*34*) and the rearrangement of disulfide intermediates in bovine pancreatic trypsin inhibitor (*35*). The positive value of $m^{\ddagger}$ for the first-order reaction argues that I_2 is an on-pathway intermediate (Scheme 1A).

Therefore, it is reasonable to conclude that I_2 is an obligatory, on-pathway intermediate. The model shown in Scheme 1A provides the most appropriate and consistent description of the folding and unfolding responses of $[2-66]_2$ TR.

Structural Details of the Folding Reaction of [2−66]$_2$ TR. Comparison of the kinetic responses of folding and unfolding by fluorescence and circular dichroism permits insight into the degree of coordination between the development of secondary, tertiary, and quaternary structures. For WT TR, these two techniques monitor similar relaxation times (*14*). The data in Figure 3B are the result of the simultaneous fitting of WT TR SF-FL and SF-CD kinetic traces to a sum of three exponentials with globally linked relaxation times. The fitted relaxation times for the first-order folding and unfolding reactions of $[2-66]_2$ TR are also similar by both spectroscopic probes (Figure 3A). Any apparent discrepancy or poor agreement may be attributed to the lower signal-to-noise ratio inherent in the SF-CD method, despite the averaging of 30−50 traces. Therefore, it can be concluded that the final development of secondary and tertiary structure of the core domain occurs in a concerted manner after dimerization.

The extent to which secondary and tertiary structures are formed in the I_2 species is, however, not equal. The CD data could only be collected at micromolar monomer concentrations, precluding direct observation of the dimerization reaction. However, at 15 °C and 7 μM monomer, the CD signal detected in the stopped-flow dead time represents ~70% of the CD amplitude for the $2U \rightleftharpoons N_2$ reaction (data not shown), implying that I_2 has ~70% of the secondary structure of N_2. At the same temperature, and monomer concentrations of 0.1−0.4 μM monomer, the $2U \rightleftharpoons I_2$ reaction was detectable by SF-FL (Figure 4). The dimerization reaction contributes only ~20% of the FL changes observed upon folding. Therefore, the dimeric intermediate possesses a majority of the native secondary structure, but only a small fraction of the solvent exclusion around Trp-19 that is seen in the fully folded $[2-66]_2$ dimer. This is supported by the ANS experiments (Figure 2B); the binding of ANS to I_2 shows that hydrophobic surfaces have formed in I_2 but are not yet excluded from solvent.

The *m* values for the $2U \rightleftharpoons I_2$ and $I_2 \rightleftharpoons N_2$ reactions provide a general measure of the amount of surface area buried, particularly hydrophobic surface (*31*). The relative *m* values for the $2U \rightleftharpoons I_2$ and $I_2 \rightleftharpoons N_2$ reactions are 1.2 and 0.78, respectively (Table 1). This suggests that ~60% of the solvent-excluded surface of the N_2 species has been buried in I_2. The dimeric intermediate must be stabilized by both the formation of a solvent-excluded hydrophobic subcore, in addition to the development of secondary structure. The small fluorescence change for Trp-19, located near the N-terminus of the A-helix (Figure 1), suggests that the majority of the side chains buried in the initial dimerization may be comprised of nonfluorescent, aliphatic residues (Leu, Ile, Val, and Met) located in the C-terminal portion of the A-helix, as well as the B and C helices. The first-order reaction represents the further burial of Trp-19 and development of additional α-helical structure to obtain the native dimeric structure of $[2-66]_2$ TR.

A dimeric intermediate has also been observed in the equilibrium thermal unfolding of $[2-66]_2$ TR at >60 °C (*25*). From global fits of CD and UV-absorbance data, it was concluded that this thermal I_2 species contains nearly all of the secondary structure of the native dimer, but practically none of the tertiary structure around the aromatic residues, particularly Trp-19. These characteristics are similar to those observed for the I_2 ensemble transiently populated during the refolding from a urea-denatured form at 25 °C.

Diffusion-Limited Association Reactions in Protein Folding. Many reactions catalyzed by enzymes have been shown to be diffusion-controlled; i.e., the formation of the enzyme−substrate complex is rate-limiting, not the subsequent chemistry (e.g., refs *36*−*38*). Diffusion-limited association reactions have been observed not only for enzymes with small molecule substrates but in protein−protein interactions as well. The bacterial toxin, colicin E9 DNase, associates with a cytosolic inhibitor, Im9, with an association rate constant of 4×10^9 M^{-1} s^{-1} (*39*). Complex formation between the *E. coli* chaperone, SecB, and unfolded bovine pancreatic trypsin inhibitor proceeds with a rate constant of 5×10^9 M^{-1} s^{-1} (*40*). The association rate of GroEL with denatured barnase is 3.5×10^7 M^{-1} s^{-1} (*41*).

These examples demonstrate that folded enzymes can associate with protein substrates or inhibitors in a diffusion-limited reaction, even when the substrate is an unfolded protein. They do not address, however, the issue of whether two partially folded polypeptides can associate in a folding reaction with a similar rate constant. Global fitting of the data at 15 °C and 1 M urea (Figure 4) gives a lower limit of $(3 \pm 1) \times 10^8$ M^{-1} s^{-1} for the second-order rate constant for $[2-66]_2$ TR. At 25 °C, this association rate constant, 7×10^8 M^{-1} s^{-1}, clearly approaches the diffusion limit. The theoretical maximal rate constant for the association of two spheres with uniform reactivity over their entire surface is $\sim 7 \times 10^9$ M^{-1} s^{-1} for a heterodimer (*42*, *43*); the rate constant for a homodimeric association would be half of this, or $\sim 3 \times 10^9$ M^{-1} s^{-1} (*44*). The efficiency of the $[2-66]_2$ TR dimerization reaction is very high; ≥1 in 4 reactions are productive and result in continued folding to the native dimer, rather than in dissociation.

Near-diffusion-limited reactions have also been observed for other protein folding systems. Tropomyosin, whose dimerization motif is a coiled-coil, associates with a rate $\geq 8 \times 10^7$ M^{-1} s^{-1} (*45*). A triple mutant of the P-22 *Arc* repressor, in which a triad of buried charged residues are replaced by nonpolar residues, dimerizes with a rate of 3×10^8 M^{-1} s^{-1} (*6*). Such rapid and efficient diffusion-limited reactions in protein folding decrease the likelihood of the unproductive aggregation of isolated monomers into dead-

end products such as inclusion bodies in the cell. Presumably, the very rapid association of chaperones such as SecB and GroEL with unfolded proteins (10^7-10^9 M^{-1} s^{-1}) is another mechanism to prevent the unproductive associations of unfolded monomers.

Two factors probably contribute to the near-diffusion-limited rate constant of $[2-66]_2$ TR. First, productive collisions may require a specific structure for the presentation of residues. If so, the second-order rate constant would depend on the fractional population of monomers that have this preassembled surface. Monomeric TR, which appears transiently during the folding of WT TR, has moderate stability, a $\Delta G°(H_2O)$ value of 3 kcal mol^{-1}, ~60% of the helical structure observed for the native dimer, and exposed hydrophobic surfaces, as deduced from ANS-binding experiments (*14*). Similarly, a mutated TR (L39E) forms a stable monomeric species with both secondary and tertiary structure (*46*, *47*). Introduction of L39E into the [2−66] TR resulted in a monomeric fragment that retained some secondary and tertiary structure (*55*). Thus monomeric forms of full-length TR and the dimerization core are capable of folding to some extent in the absence of a partner chain, potentially enhancing the observed refolding rate. A contrasting example is provided by the coiled-coil GCN4-p1 peptides, which dimerize with a rate constant of 4×10^5 M^{-1} s^{-1} at 5 °C, with no detectable transiently populated monomeric species (*27*).

A second factor likely to be involved in the efficient association of *Trp* repressor monomers is the nonspecific interaction between exposed hydrophobic surfaces on 2-folded monomers. Precedent for this supposition is provided by the non-sequence-specific hydrophobic interaction observed for chaperonins, such as GroEL or SecB, which can associate with unfolded or partially folded proteins with rates of 10^7 to 10^9 M^{-1} s^{-1}. Although it is impossible to detect a transient monomeric form of [2−66] TR by stopped-flow methods and determine its secondary structure content and ability to bind ANS, the properties of monomeric full-length TR make it reasonable to conclude that nonpolar surfaces enhance dimerization efficiency in the folding of the dimeric TR variants.

Implications for the Folding of WT TR. The simple folding mechanism of $[2-66]_2$ TR provides insights into the cause of the multiple channels of the WT TR folding mechanism (described in Introduction). The contrasting mechanisms imply that the DNA reading heads are responsible for the complexity observed for the full-length protein. The parallel pathways of WT TR appear to arise from alternative interactions of the three C-terminal helices with the hydrophobic core. The simple folding mechanism of $[2-66]_2$ TR (Scheme 1A) demonstrates that the complex, intertwined topology of the dimer interface (Figure 1) does not necessitate a complicated refolding response or inefficient association.

The $I_2 \rightleftharpoons N_2$ reaction of $[2-66]_2$ TR may be analogous to the isomerization of the transiently populated dimeric intermediates in the folding of the full-length protein. In WT TR, these reactions have $m^‡$ values of ~0 (Figure 3B, 1−2.5 M urea), whereas the $m^‡$ value for the core is ~0.6 (Figure 3A). A possible explanation is that the three C-terminal helices of WT TR, absent in $[2-66]_2$ TR, may contribute to the buried hydrophobic area in the dimeric intermediates of WT. By excluding from solvent the surfaces that are rearranged in the $I_2 \rightarrow N_2$ reactions, further folding would proceed with a very low $m^‡$ value.

From the perspective of an energy landscape (*48*, *49*), the folding of WT TR is consistent with a rough energy surface with multiple trajectories from unfolded monomer to native dimer. The folding of $[2-66]_2$ TR, by contrast, can be described by a relatively smooth energy surface with only two barriers which all of the unfolded protein must traverse.

ACKNOWLEDGMENT

We appreciate Dr. Osman Bilsel's efforts in the development of the in-house global fitting routines and his assistance in their utilization. We are indebted to Drs. Jill A. Zitzewitz and Osman Bilsel for many fruitful discussions. We also thank Dr. Ira Ropson at the Hershey Medical Center of the Pennsylvania State University for the use of his Applied Photophysics SF-FL.

REFERENCES

1. Matthews, C. R. (1993) *Ann. Rev. Biochem. 62*, 653−683.
2. Fersht, A. R. (1995) *Proc. Natl. Acad. Sci. U.S.A. 92*, 10869−10873.
3. Shortle, D., Wang, Y., Gillespie, J. R., and Wrabl, J. O. (1996) *Protein Sci. 5*, 991−1000.
4. Jaenicke, R. (1987) *Prog. Biophys. Mol. Biol. 49*, 117−237.
5. Milla, M. E., and Sauer, R. T. (1994) *Biochemistry 33*, 1125−1133.
6. Waldburger, C. D., Jonsson, T., and Sauer, R. T. (1996) *Proc. Natl. Acad. Sci. U.S.A. 93*, 2629−2634.
7. Planchenault, T., Navon, A., Schulze, A. J., and Goldberg, M. E. (1995) *Eur. J. Biochem. 240*, 615−621.
8. Gast, K., et al. (1997) *Protein Sci. 6*, 2578−2588.
9. Gittelman, M. S., and Matthews, C. R. (1990) *Biochemistry 29*, 7011−7020.
10. Reedstrom, R. J., and Royer, C. A. (1995) *J. Mol. Biol. 253*, 266−276.
11. Eftink, M. R., Helton, K. J., Beavers, A., and Ramsay, G. D. (1994) *Biochemistry 33*, 10220−10228.
12. Zhang, R.-G., et al. (1987) *Nature 327*, 591−597.
13. Zhao, D., Arrowsmith, C. H., Jia, X., and Jardetzky, O. (1993) *J. Mol. Biol. 229*, 735−746.
14. Mann, C. J., and Matthews, C. R. (1993) *Biochemistry 32*, 5282−5290.
15. Mann, C. J., Xiao, S., and Matthews, C. R. (1995) *Biochemistry 34*, 14573−14580.
16. Perham, R. N. (1995) *Methods Enzymol. 251*, 436−448.
17. Maurer, P., et al. (1995) *J. Mol. Biol. 253*, 347−357.
18. Ko, Y. H., Thomas, P. J., and Pederson, P. L. (1994) *J. Biol. Chem. 269*, 14584−14588.
19. Kippen, A. D., Sancho, J., and Fersht, A. R. (1994) *Biochemistry 33*, 3778−3786.
20. Kippen, A. D., and Fersht, A. R. (1995) *Biochemistry 34*, 1464−1468.
21. Ruiz-Sanz, J., de Prat Gay, G., Otzen, D. E., and Fersht, A. R. (1995) *Biochemistry 34*, 1695−1701.
22. Gegg, C. V., Bowers, K. E., and Matthews, C. R. (1996) *A general approach for the design and isolation of protein fragments: The molecular dissection of dihydrofolate reductase*, Techniques in Protein Chemistry, (Marshak, D., Ed.) Vol. VII, pp 439−448, Academic Press, San Diego.
23. Gegg, C. V., Bowers, K. E., and Matthews, C. R. (1997) *Protein Sci. 6*, 1885−1892.
24. Tasayco, M. L., and Carey, J. (1992) *Science 255*, 594−597.
25. Gloss, L. M., and Matthews, C. R. (1997) *Biochemistry 36*, 5612−5623.
26. Pulah, J. L., and Yanofsky, C. (1986) *Nucleic Acids Res. 14*, 7851−7860.
27. Zitzewitz, J. A., Bilsel, O., Luo, J., Jones, B. E., and Matthews, C. R. (1995) *Biochemistry 34*, 12812−12819.
28. Matthews, C. R. (1987) *Methods Enzymol. 154*, 498−511.

29. Engelhard, M., and Evans, P. A. (1995) *Protein Sci. 4*, 1553−1562.
30. Kuwajima, K., Garvey, E. P., Finn, B. E., Matthews, C. R., and Sugai, S. (1991) *Biochemistry 30*, 7693−7703.
31. Myers, J. K., Pace, C. N., and Scholtz, J. M. (1995) *Protein Sci. 4*, 2138−2148.
32. Kiefhaber, T. (1995) *Proc. Natl. Acad. Sci. U.S.A. 92*, 9029−9033.
33. Tanford, C. (1970) *Adv. Protein Chem. 24*, 1−95.
34. Sosnick, T. R., Mayne, L., and Englander, S. W. (1996) *Proteins 24*, 413−426.
35. Weissman, J. S., and Kim, P. S. (1995) *Nat. Struct. Biol. 2*, 1123−1130.
36. Albery, W. J., and Knowles, J. R. (1976) *Biochemistry 15*, 5631−5640.
37. Brouwer, A. C., and Kirsch, J. F. (1982) *Biochemistry 21*, 1302−1307.
38. Hardy, L. W., and Kirsch, J. F. (1984) *Biochemistry 23*, 1275−1282.
39. Wallis, R., Moore, G. R., James, R., and Kleanthous, C. (1995) *Biochemistry 34*, 13743−13750.
40. Fekkes, P., den Blaauwen, T., and Driessen, A. J. M. (1995) *Biochemistry 34*, 10078−10085.
41. Corrales, F. J., and Fersht, A. R. (1995) *Proc. Natl. Acad. Sci. U.S.A. 92*, 5326−5330.
42. Fersht, A. R. (1985) *Enzyme Structure and Mechanisms*, W. H. Freeman, New York.
43. Janin, J. (1997) *Proteins 28*, 153−161.
44. Amdur, I., and Hammes, G. G. (1966) *Chemical Kinetics: Principles and Selected Topics*, McGraw-Hill, New York.
45. Mo, J., Holtzer, M. E., and Holtzer, A. (1991) *Proc. Natl. Acad. Sci. U.S.A. 88*, 916−920.
46. Shao, X., Hensley, P., and Matthews, C. R. (1997) *Biochemistry 36*, 9941−9949.
47. Shao, X., and Matthews, C. R. (1998) *Biochemistry 37*, 7850−7858.
48. Bryngelson, J. D., Onuchic, J. N., Socci, N. D., and Wolynes, P. G. (1995) *Proteins 21*, 167−195.
49. Wolynes, P. G., Onuchic, J. N., and Thirumalai, D. (1995) *Science 267*, 1619−1620.
50. Royer, C. A., Mann, C. J., and Matthews, C. R. (1993) *Protein Sci. 2*, 1844−1852.
51. Horn, R. A., and Johnson, C. R. (1985) *Matrix Analysis*, Cambridge University Press, Cambridge, U.K.
52. Henry, E. R., and Hofrichter, J. (1992) *Methods Enzymol. 210*, 129−193.
53. Golub, G., and VanLoan, C. (1983) *Matrix Computations*, Johns Hopkins University Press, Baltimore, MD.
54. Kraulis, P. J. (1991) *J. Appl. Crystallogr. 24*, 946−950.
55. Shao, X., and Matthews, C. R. Unpublished results.

BI981511P